

## Investigation of the reactions of small neutral iron oxide clusters with methanol

Yan Xie, Feng Dong, Scott Heinbuch, Jorge J. Rocca, and Elliot R. Bernstein\*

Citation: *The Journal of Chemical Physics* **130**, 114306 (2009); doi: 10.1063/1.3086724

View online: <http://dx.doi.org/10.1063/1.3086724>

View Table of Contents: <http://aip.scitation.org/toc/jcp/130/11>

Published by the *American Institute of Physics*

---

---

**COMPLETELY  
REDESIGNED!**



**PHYSICS  
TODAY**

*Physics Today* Buyer's Guide  
Search with a purpose.

## Investigation of the reactions of small neutral iron oxide clusters with methanol

Yan Xie,<sup>1,2</sup> Feng Dong,<sup>1,2</sup> Scott Heinbuch,<sup>2,3</sup> Jorge J. Rocca,<sup>2,3</sup> and Elliot R. Bernstein<sup>1,2,a)</sup>

<sup>1</sup>Department of Chemistry, Colorado State University, Fort Collins, Colorado 80523, USA

<sup>2</sup>NSF ERC for Extreme Ultraviolet Science and Technology, Colorado State University, Fort Collins, Colorado 80523, USA

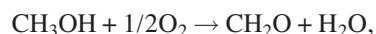
<sup>3</sup>Department of Electrical and Computer Engineering, Colorado State University, Fort Collins, Colorado 80523, USA

(Received 5 September 2008; accepted 2 February 2009; published online 20 March 2009)

Reactions of neutral iron oxide clusters ( $\text{Fe}_m\text{O}_n$ ,  $m=1-2$ ,  $n=0-5$ ) with methanol ( $\text{CH}_3\text{OH}$ ) in a fast flow reactor are investigated by time of flight mass spectrometry. Detection of the neutral iron oxide cluster distribution and reaction intermediates and products is accomplished through single photon ionization by a 118 nm (10.5 eV) VUV laser. Partially deuterated methanol ( $\text{CD}_3\text{OH}$ ) is employed to distinguish reaction products and reaction mechanisms. Three major reactions are identified experimentally:  $\text{CH}_3\text{OH}$  association with  $\text{FeO}$ ; methanol dehydrogenation on  $\text{FeO}_{1,2}$  and  $\text{Fe}_2\text{O}_{2-5}$ ; and  $(\text{CH}_2\text{O})\text{Fe}$  formation. Density functional theory calculations are carried out to identify reaction products, and to explore the geometric and electronic structures of the iron oxide clusters, reaction intermediates, and transition states, and to evaluate reaction pathways. Neutral formaldehyde is calculated to be formed on  $\text{FeO}_{1,2}$  and  $\text{Fe}_2\text{O}_{2-5}$  clusters. Hydrogen transfer from methanol to iron oxide clusters occurs first from the O–H moiety of methanol, and is followed by a hydrogen transfer from the C–H moiety of methanol. Computational results are in good agreement with experimental observations and reveal reaction mechanisms for neutral iron oxide clusters taking methanol to formaldehyde through various reaction intermediates. Based on the experimental results and the calculated reaction mechanisms and pathways, complete catalytic cycles are suggested for the heterogeneous reaction of  $\text{CH}_3\text{OH}$  to  $\text{CH}_2\text{O}$  facilitated by an iron oxide catalyst. © 2009 American Institute of Physics. [DOI: 10.1063/1.3086724]

### I. INTRODUCTION

Transition metal oxides are widely used as heterogeneous catalysts in the chemical industry, and their reactive behavior has been extensively studied.<sup>1-3</sup> Methanol as a clean energy resource can be used directly for transportation or added in the conventional fossil fuels.<sup>4,5</sup> Commercially, methanol is synthesized from carbon monoxide and hydrogen on a mixture of copper oxide and zinc oxide supported by alumina,<sup>6,7</sup> and almost 40% of the produced methanol is converted to formaldehyde over iron molybdenum oxide catalysts.<sup>8-10</sup> The reaction enthalpy for methanol selective oxidation to formaldehyde is<sup>11</sup>



$$\Delta H = -153 \text{ kJ/mol}.$$

Dehydrogenation of methanol over transition metal oxides in the gas phase has been extensively investigated; most researchers focus on the reactions of cation or anion metal oxide clusters because charged particles can be readily manipulated by electric and magnetic fields. Charged metal and metal oxide clusters can be selected and reacted individually under well defined conditions, and reaction products can be identified from independent, mass selected, charged par-

ticles. Most work is performed by time of flight mass spectrometry (TOFMS) or Fourier-transform ion cyclotron resonance mass spectrometry (FTICRMS). Neutral metal oxide clusters, on the other hand, cannot be mass selected presently, and must be ionized for detection. Methanol dehydrogenation oxidation on  $\text{V}_m\text{O}_n^+$ ,<sup>12(a)-12(c),13(a)</sup>  $\text{Mo}_x\text{O}_y^+$ ,<sup>14</sup>  $\text{FeO}^+$ ,<sup>12(d),15(a)</sup>  $\text{FeO}^{2+}$ ,<sup>16</sup>  $\text{MO}^+$  ( $M=\text{V}, \text{Nb}, \text{Ta}$ ),<sup>17</sup>  $\text{NbO}^-$ ,<sup>18</sup>  $\text{M}_x\text{O}_y^-$  ( $M=\text{Mn}, \text{Fe}, \text{Co}, \text{Ni}, \text{Cu}$ ) (Ref. 19) has been explored experimentally and theoretically, and products are recognized as formaldehyde, hydrogen, water, etc. Only a few studies concentrate on neutral species, mostly through theoretical calculations<sup>20-22,23(a)</sup> and condensed phase studies.<sup>24,25</sup> To date, no experimental results for methanol dehydrogenation on neutral metal oxide clusters have been reported, however.

Iron oxide is a common heterogeneous catalyst for many catalytic processes because it is abundantly distributed around the earth's surface.  $\text{Fe}_3\text{O}_4$  is used for catalytic reactions such as the Haber process (ammonia synthesis from nitrogen and hydrogen) (Ref. 26) and the water gas shift reaction.<sup>27,28</sup> Recently, iron oxide cluster reactivity in the gas phase has attracted researchers' attention because it can be used to replace noble metal and metal oxides, especially, for CO oxidation to  $\text{CO}_2$ .

Iron oxide cluster geometric structures and properties,<sup>29-35</sup> as well as reactivity,<sup>12,13(b)-13(d),15,16,19,23,36-39</sup> have been demonstrated by various groups. Reilly *et al.* stud-

<sup>a)</sup>Author to whom correspondence should be addressed. Electronic mail: erb@lamar.colostate.edu.

ied the reactivity of  $\text{Fe}_{1-2}\text{O}_{\leq 6}^-$ ,<sup>13(c)</sup>  $\text{Fe}_{1-2}\text{O}_{1-5}^+$ ,<sup>13(d)</sup> and  $\text{FeO}_3^{+/-}$  [Ref. 13(b)] clusters with CO experimentally and theoretically; all charged (cationic and anionic) clusters in their studies are reacted with CO and the most active anion clusters are composed of one more oxygen atom than iron atom; however, observation of reactions of neutral iron oxide clusters ( $\text{Fe}_{1,2}\text{O}_{\leq 5}$ ) with CO by Xue *et al.*<sup>40(a)</sup> indicate that  $\text{FeO}_{2,3}$  species have high reactivity toward CO, whereas FeO and  $\text{Fe}_2\text{O}_{4,5}$  species have low or no reactivity toward CO. DFT calculations for reaction barriers and mechanisms further confirm these experimental results. Comparison of neutral and charged cluster studies suggests that a charge on the cluster surface significantly affects cluster reactivity, especially for small clusters. Reaction of  $\text{FeO}^+$  with methanol has been reported by Schröder *et al.* in 1996.<sup>12(d)</sup> Four types of reactions, (1)  $\text{FeO}^+ + \text{CH}_3\text{OH} \rightarrow (\text{CH}_2\text{O})\text{FeOH}^+ + \text{H}^-$ , (2)  $\text{FeO}^+ + \text{CH}_3\text{OH} \rightarrow (\text{CH}_2\text{O})\text{Fe}^+ + \text{H}_2\text{O}$ , (3)  $\text{FeO}^+ + \text{CH}_3\text{OH} \rightarrow (\text{H}_2\text{O})\text{Fe}^+ + \text{CH}_2\text{O}$ , and (4)  $\text{FeO}^+ + \text{CH}_3\text{OH} \rightarrow \text{Fe}^+ + \text{CH}_2\text{O} + \text{H}_2\text{O}$ , are identified, with the first two reactions dominant. The reaction enthalpies for these reactions are estimated by thermochemical data to be  $-0.48$ ,  $-2.04$ ,  $-1.95$ , and  $-0.61$  eV, respectively. Yoshizawa and Kagawa<sup>15(a)</sup> calculated the reaction pathways for reaction of  $\text{FeO}^+ + \text{CH}_3\text{OH}$  at the B3LYP/6-311G\*\* level of theory, and three different paths are proposed, and two of these are competitive in energy. Hydrogen transfer from the O–H group and from the C–H group of methanol is involved in these latter two pathways. Additionally,  $\text{FeO}_2^-$ ,  $\text{FeO}_3^-$ ,  $\text{Fe}_2\text{O}_3^-$ , and  $\text{Fe}_2\text{O}_4^-$  have been investigated for reactions with methanol by Oliveira *et al.*<sup>19</sup> using FTICRMS, and the reaction efficiency order of these species is suggested to be  $\text{FeO}_2^- > \text{Fe}_2\text{O}_3^- > \text{Fe}_2\text{O}_4^-$ , whereas  $\text{FeO}_3^-$  has no reactivity toward methanol. Calculations for reactions of  $\text{FeO}^{2+}$  with methanol in the gas phase and in water have been performed recently by Louwse *et al.*,<sup>16</sup> and two reaction mechanisms, C–H bond activation followed by O–H bond activation and O–H bond activation followed by C–H bond activation, are explored. The first step of the reaction involves C–H bond activation by  $\text{FeO}^{2+}$ , according to their DFT calculations.

An ideal ionization source for neutral clusters should have a single photon energy around 10 eV to ionize the reactants, intermediates, and products associated with metal oxide cluster reactions, in order to avoid severe neutral cluster fragmentation. Recently, a 118 nm (10.5 eV) VUV laser and a 46.9 nm (26.5 eV) x-ray laser have been developed for study of neutral transition metal oxide cluster distributions, growth dynamics, and reactivity.<sup>40</sup>  $\text{Fe}_m\text{O}_n$ ,<sup>40(b)</sup>  $\text{Cu}_m\text{O}_n$ ,<sup>40(c)</sup>  $\text{Zr}_m\text{O}_n$ ,<sup>40(d)</sup>  $\text{Ti}_m\text{O}_n$ ,<sup>40(e)</sup>  $\text{V}_m\text{O}_n$ ,<sup>40(f),40(g),40(i),40(j)</sup>  $\text{Ta}_m\text{O}_n$ ,<sup>40(g)</sup>  $\text{Nb}_m\text{O}_n$ ,<sup>40(g)</sup>  $\text{V}_m\text{S}_n$ ,<sup>40(h)</sup> and  $\text{Si}_m\text{O}_n$  [Ref. 40(k)] clusters are generated by laser ablation and ionized by 118 or 46.9 nm laser radiations, and their reactivity further investigated. In this paper, reactions of neutral iron oxide clusters with methanol are studied by 118 nm single photon ionization (SPI) coupled with TOFMS. Partially deuterated methanol ( $\text{CD}_3\text{OH}$ ) is additionally employed for comparison with  $\text{CH}_3\text{OH}$  reactant to identify reaction products. Detailed reaction mechanisms are suggested based on the experimental observations and DFT calculations. Based on the combined

experimental and theoretical results, we present a proposed mechanism for the partial oxidation of methanol to formaldehyde facilitated by an iron oxide catalyst.

## II. METHODS

### A. Experimental procedures

The experimental setup for laser ablation coupled with a fast flow reactor has been described previously in detail.<sup>40(i),40(m)</sup> A brief summary of the apparatus is given below.  $\text{Fe}_m\text{O}_n$  clusters are generated by reaction of laser ablated iron foil (99.9%, Sigma Aldrich, 0.1 mm thickness) with 5%  $\text{O}_2$  seeded in a helium carrier gas (99.99%, General Air). A 10 Hz, focused, 532 nm  $\text{Nd}^{3+}$ :YAG laser ( $\text{Nd}^{3+}$ :yttrium aluminum garnet) with 7 mJ/pulse energy is used for the laser ablation. The ablation occurs at the exit of a pulse nozzle (R. M. Jordan, Co.) with a backing gas pressure of typically 70 psi. Clusters are generated in a stainless steel channel, 1.8 mm diameter by 19 mm length. The ablated Fe plasma reacts with the backing gas to form  $\text{Fe}_m\text{O}_n$  clusters. These clusters are cooled by the ensuing expansion and are reacted with reactant gases in a directly coupled fast flow reactor. The reactor is 6.3 mm diameter by 76 mm length. The reactant gases, methanol (99.9% Sigma Aldrich) seeded in a pure helium gas, with a 20 psi backing pressure, are injected into the reactor by a pulsed general valve (Parker, Serial 9). The concentration of methanol in the helium gas is estimated as 12%. The delay time between the Jordan valve and the general valve openings is optimized for the best product generation. The pressure in the fast flow reactor can be estimated at 14 Torr when the reactant gases are introduced into the reactor. The  $\text{Fe}_m\text{O}_n$  clusters collide with the  $\text{CH}_3\text{OH}$  and helium bath gas in the reactor; the collision rate for iron oxide clusters with helium is estimated  $\sim 10^8 \text{ s}^{-1}$ .<sup>40(a)</sup> After the reaction,  $\text{Fe}_m\text{O}_n$  clusters are thermalized to  $\sim 300\text{--}400$  K by collision<sup>41</sup> and the  $\text{Fe}_m\text{O}_n$  clusters, reactants and products, are further expanded and cooled. An electric field is placed downstream of the reactor in order to remove any residual ions from the molecular beam. The beam of neutral reactants and products are skimmed into a second chamber and ionized by a separated VUV laser (118 nm, 10.5 eV). 118 nm laser radiation is generated by focusing the third harmonic (355 nm,  $\sim 30$  mJ/pulse) of a  $\text{Nd}^{3+}$ :YAG laser in a tripling cell filled with  $\sim 250$  Torr argon/xenon mixed gas (the ratio is Ar:Xe=10:1). A magnesium fluoride prism (Crystaltechno LTD, Russia, 6° apex angle) is inserted into the laser beam to enhance separation of the 118 nm beam from the 355 nm input beam. The 118 nm laser intensity is about  $1 \mu\text{J}/\text{cm}^2$ . Photoions are detected by a TOFMS and signals are amplified (HFAC-26dB, Becker & Hickl GmbH) and typically averaged for 2500 laser pulses by a digital storage oscilloscope (Tektronix 5032B, USA), as described before.<sup>40(i),40(m)</sup>

### B. Computational procedures

Calculations of the reactions of  $\text{Fe}_m\text{O}_n$  clusters with methanol are performed by density functional theory (DFT) within the GAUSSIAN 03 program package.<sup>42</sup> The potential energy surfaces (PESs) for the reaction of  $\text{FeO}_n$  with metha-

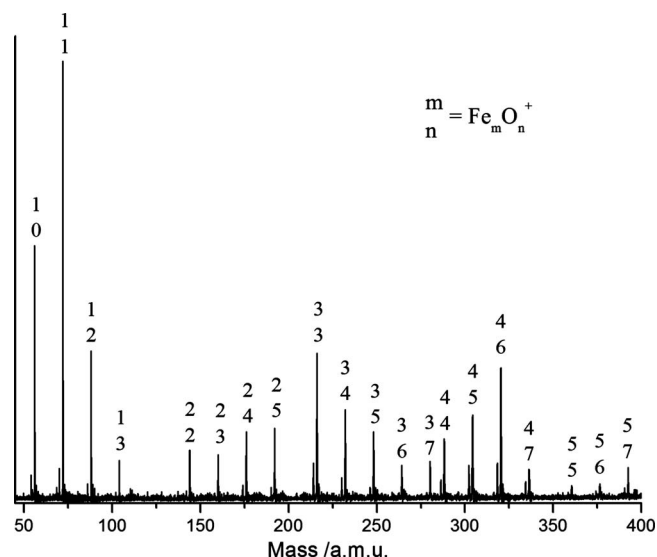


FIG. 1. Neutral iron oxide cluster distribution ionized by 118 nm laser radiation.

not involve geometry optimizations of the reactants, reaction intermediates, transition states, and products. Energies, at 0 K, including zero point energy (ZPE) corrections, are adopted to calculate the reaction pathways. Vibrational frequency calculations are further investigated to determine the stable structures and the transition states, which have zero and one imaginary frequency, respectively. In addition, intrinsic reaction coordinate (IRC) calculations are carried out to confirm that a specific transition state connects two appropriate reaction intermediates along the reaction pathways. The Becke three parameter Lee–Yang–Parr exchange–correlation functional (B3LYP), coupled with the triple split 6-311+G(*d*) basis set, is adopted for all iron, oxygen, carbon, and hydrogen atoms. The same calculational methods have been successfully applied for the study of the reaction of  $\text{Fe}_m\text{O}_n$  clusters with CO.<sup>40(a)</sup>

### III. RESULTS

#### A. Experimental results

Figure 1 present a neutral iron oxide cluster distribution with 5%  $\text{O}_2/\text{He}$  carrier gas generated through 118 nm laser ionization. In this condition, only  $\text{Fe}_m\text{O}_n$  ( $n \geq m$ ) clusters are observed in the mass spectrum, such as  $\text{FeO}_{0-3}$ ,  $\text{Fe}_2\text{O}_{2-5}$ ,  $\text{Fe}_3\text{O}_{3-6}$ ,  $\text{Fe}_4\text{O}_{4-7}$ , and  $\text{Fe}_5\text{O}_{5-7}$ . This spectrum is slightly different from our previous investigation, in which both  $\text{Fe}_m\text{O}_n$  clusters ( $n > m$ ,  $n = m$ , and  $n < m$ ) are all observed.<sup>40(b)</sup> These two sets of experimental conditions are not the same, however, in the previous experiment a 20 psi 0.75%  $\text{O}_2/\text{He}$  mixture gas is employed for the carrier gas and cluster generation/ionization takes place in a single chamber in which the distance from laser ablation to ionization is about 10 cm. In contrast, the high oxygen concentration of the 70 psi backing gas used in this work generates more highly oxidized  $\text{Fe}_m\text{O}_n$  clusters. The total ion signal intensity is lower than that for our previous report by approximately a factor of 30;<sup>40(b)</sup> however, since the distance from laser ablation to TOFMS ionization is 44 cm in this two chamber

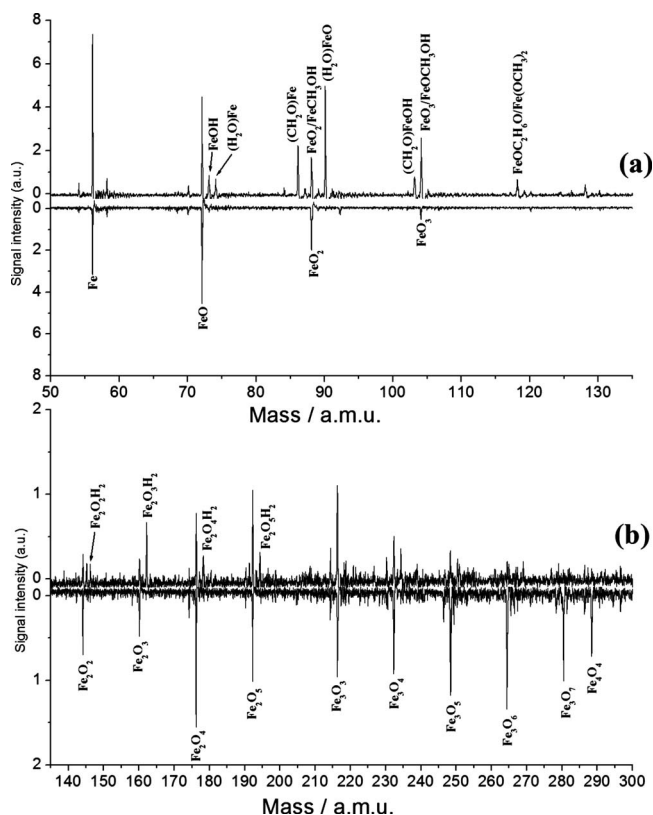


FIG. 2. Product distribution for the reaction of neutral iron oxide clusters with pure helium (bottom panel) and methanol seeded in helium (top panel) in a fast flow reactor. Panel (a) presents the low mass region and panel (b) presents the high mass region.

configuration, compared to 10 cm in our previous report, and since  $I \propto 1/d^2$  ( $I$ : signal intensity,  $d$ : distance from ablation to ionization), this decrease in signal intensity is to be expected. A 118 nm ionization laser is employed to generate ions for detection, as described in the experimental section, and thus, all the mass peaks in Fig. 1 are symmetrical and their line-widths are identical ( $\sim 10$  ns). These facts clearly show that the 335 nm, multiphoton, and thus fragmenting, contribution to the ionization and mass spectra, is negligible.

Mass spectra generated for the reaction of neutral iron oxide clusters with  $\text{CH}_3\text{OH}$  seeded in the helium gas in a fast flow reactor are presented in Fig. 2. Pure helium in the fast flow reactor at  $\sim 14$  Torr as a reference is further investigated and the mass spectra determined from this experiment are shown as the bottom patterns in Fig. 2. The products of reactions of  $\text{Fe}_m\text{O}_n$  with methanol and partially deuterated methanol are listed in Table I.

#### B. Calculational results

Reaction energies involving the reactions of iron oxide clusters with methanol presented in Fig. 2 and Table I are calculated by DFT: four dominant types of reactions are considered and summarized below.

- (1) Association reactions ( $\text{Fe}_m\text{O}_n + \text{CH}_3\text{OH} \rightarrow \text{Fe}_m\text{O}_n\text{CH}_3\text{OH}$ ). Since the mass number of  $\text{CH}_3\text{OH}$ , 32 amu, is equal to that of  $\text{O}_2$ , one cannot distinguish the reactant  $\text{Fe}_m\text{O}_n$  from the product  $\text{Fe}_m\text{O}_{n-2}\text{CH}_3\text{OH}$  in

TABLE I. Observed product for the reactions of neutral iron oxide clusters with CH<sub>3</sub>OH and CD<sub>3</sub>OH.

Mass	CH <sub>3</sub> OH	Mass	CD <sub>3</sub> OH
73	FeOH	... <sup>a</sup>	...
74	HFeOH	75	FeOHD
86	(CH <sub>2</sub> O)Fe	88	(CD <sub>2</sub> O)Fe <sup>b</sup>
90	(H <sub>2</sub> O)FeO	91	(HDO)FeO
103	(CH <sub>2</sub> O)FeOH <sup>a</sup>	... <sup>a</sup>	...
104	FeOCH <sub>3</sub> OH <sup>c</sup>	107	FeOCD <sub>3</sub> OH
118	FeOC <sub>2</sub> H <sub>6</sub> O <sup>d</sup>	124	FeOC <sub>2</sub> D <sub>6</sub> O
145	Fe <sub>2</sub> O <sub>2</sub> H	... <sup>a</sup>	...
146	Fe <sub>2</sub> O <sub>2</sub> H <sub>2</sub>	147	Fe <sub>2</sub> O <sub>2</sub> HD
162	Fe <sub>2</sub> O <sub>3</sub> H <sub>2</sub>	163	Fe <sub>2</sub> O <sub>3</sub> HD
178	Fe <sub>2</sub> O <sub>4</sub> H <sub>2</sub>	179	Fe <sub>2</sub> O <sub>4</sub> HD
194	Fe <sub>2</sub> O <sub>5</sub> H <sub>2</sub>	195	Fe <sub>2</sub> O <sub>5</sub> HD

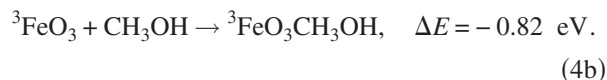
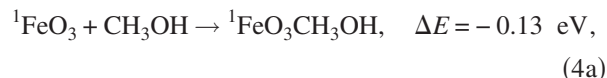
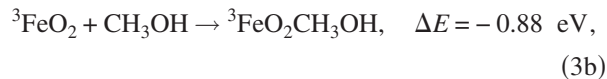
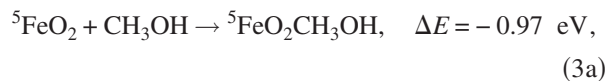
<sup>a</sup>The related deuterated species signals are too weak to be positively identified.

<sup>b</sup>Overlapped with FeO<sub>2</sub> in mass number.

<sup>c</sup>Overlapped with FeO<sub>3</sub> in mass number.

<sup>d</sup>Overlapped with FeO<sub>2</sub>CH<sub>2</sub>O in mass number.

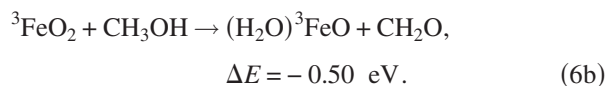
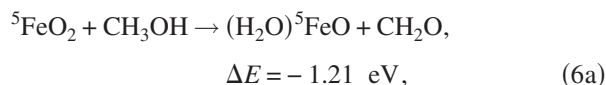
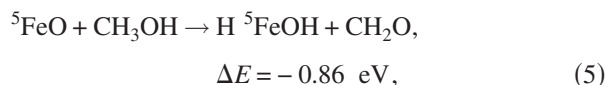
the mass spectra of Fig. 2. In addition, for the isotopic reaction of Fe<sub>m</sub>O<sub>n</sub> with CD<sub>3</sub>OH, the mass peaks Fe<sub>m</sub>O<sub>n</sub>CD<sub>3</sub>OH are also overlapped with those of Fe<sub>m</sub>O<sub>n+2</sub>HD: this latter feature comes from the neutral formaldehyde elimination reaction, Fe<sub>m</sub>O<sub>n+2</sub>+CD<sub>3</sub>OH → Fe<sub>m</sub>O<sub>n+2</sub>HD+CD<sub>2</sub>O. The association reaction energies for FeO<sub>n</sub> (n=0–3) with methanol are calculated at the B3LYP/6-311+G(d) level as



FeO, FeO<sub>2</sub>, and triplet FeO<sub>3</sub> have relatively strong association energies with methanol (1.01, 0.97/0.88, and 0.82 eV, respectively), whereas Fe and singlet FeO<sub>3</sub> have considerably weaker association energies (0.25 and 0.13 eV, respectively) based on DFT calculations. Considering that the intensity of mass peak 104 amu, corresponding to FeO<sub>3</sub> and FeOCH<sub>3</sub>OH, increases significantly after reaction and that FeO<sub>3</sub> cannot be generated from other iron oxide clusters, one can conclude that at least FeOCH<sub>3</sub>OH is clearly observed in the fast flow reactor. Since the association energy of <sup>53</sup>FeO<sub>2</sub>

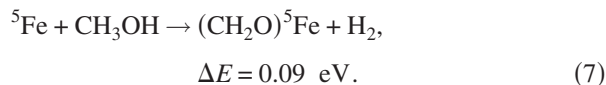
with methanol (0.97/0.88 eV) is close to that of FeO with methanol (1.01 eV), FeO<sub>2</sub>CH<sub>3</sub>OH is probably also formed in the reactor. These latter features are not observed in Fig. 2 because the overall signals are quite weak. FeCH<sub>3</sub>OH and FeO<sub>3</sub>CH<sub>3</sub>OH cannot be positively identified for the following reasons: (1) the association energy is small (0.25 and 0.13 eV for singlet FeO<sub>3</sub>); (2) the FeO<sub>3</sub> signal intensity is weak; and 3. the mass peak of FeCH<sub>3</sub>OH is overlapped with that of FeO<sub>2</sub> and the mass peak of FeOCD<sub>3</sub>OH is overlapped with that of FeO<sub>3</sub>HD.

- (2) Neutral formaldehyde elimination reaction. (Fe<sub>m</sub>O<sub>n</sub>+CH<sub>3</sub>OH → Fe<sub>m</sub>O<sub>n</sub>H<sub>2</sub>+CH<sub>2</sub>O, Fe<sub>m</sub>O<sub>n</sub>=FeO<sub>1,2</sub>, Fe<sub>2</sub>O<sub>2-5</sub>) such as

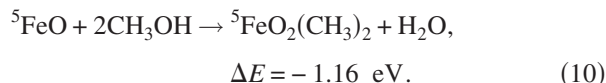
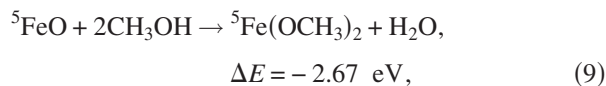
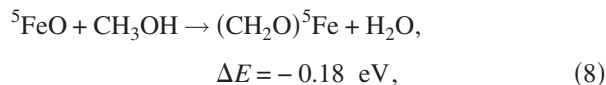


As listed in Table I, the deuterated product (HDO)FeO is observed in the reaction with CD<sub>3</sub>OH, which indicates the two hydrogen atoms in (HDO)FeO come from both the O–H and the C–H groups. CH<sub>2</sub>O has an ionization energy of 10.88 eV,<sup>11</sup> and 118 nm (10.5 eV) laser cannot ionize the neutral formaldehyde molecules through SPI. Thus, no CH<sub>2</sub>O (30 amu) are observed in the mass spectra.

- (3) Methanol dehydrogenation reaction.



- (4) Neutral water elimination.



The mass peak [FeC<sub>2</sub>H<sub>6</sub>O<sub>2</sub>] also overlaps with the product (CH<sub>2</sub>O)FeO<sub>2</sub>, however, no (CD<sub>2</sub>O)FeO<sub>2</sub> is observed for the reaction of Fe<sub>m</sub>O<sub>n</sub> with CD<sub>3</sub>OH. The structure of the product [FeC<sub>2</sub>H<sub>6</sub>O<sub>2</sub>] based on the mass spectra for the reaction of Fe<sub>m</sub>O<sub>n</sub> with methanol and deuterated methanol is unknown (Fig. 2 and Table I); both products Fe(OCH<sub>3</sub>)<sub>2</sub> and FeO<sub>2</sub>(CH<sub>3</sub>)<sub>2</sub> can be generated exothermically from methanol dehydrogenation with reaction energies of –2.67 and

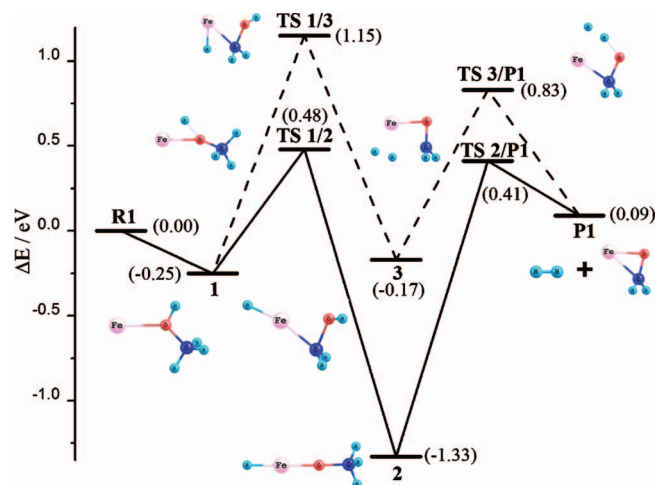


FIG. 3. (Color) Reaction pathways for  ${}^5\text{Fe}+\text{CH}_3\text{OH}\rightarrow(\text{CH}_2\text{O})^5\text{Fe}+\text{H}_2$  calculated at the B3LYP/6-311+G(*d*) level. Energies, including ZPE corrections, are given in eV and are relative to the initial energy of the  ${}^5\text{Fe}+\text{CH}_3\text{OH}$  reactants. The solid line indicates hydrogen transfer from the O–H group followed by that from the C–H group (pathway A), and the dashed line indicates hydrogen transfer from the C–H group followed by that from the O–H group (pathway B). R1:  ${}^5\text{Fe}+\text{CH}_3\text{OH}$ ; P1:  $(\text{CH}_2\text{O})^5\text{Fe}+\text{H}_2$ . Iron, oxygen, carbon, and hydrogen are in pink, red, dark blue, and light blue, respectively.

–1.16 eV, respectively. DFT calculations for the PESs may help interpret the detailed reaction mechanisms and structures for reactions (9) and (10).

The PESs and geometry structure parameters calculated by DFT for the reactions  ${}^5\text{Fe}+\text{CH}_3\text{OH}\rightarrow(\text{CH}_2\text{O})^5\text{Fe}+\text{H}_2$ ,  ${}^5\text{FeO}+\text{CH}_3\text{OH}\rightarrow(\text{CH}_2\text{O})^5\text{Fe}+\text{H}_2\text{O}$ ,  ${}^5\text{FeO}+\text{CH}_3\text{OH}\rightarrow\text{H}^5\text{FeOH}+\text{CH}_2\text{O}$ , and  ${}^{3/5}\text{FeO}_2+\text{CH}_3\text{OH}\rightarrow(\text{H}_2\text{O})^{3/5}\text{FeO}+\text{CH}_2\text{O}$  are presented in Figs. 3–7. The most stable adsorption structures are for the oxygen atom of methanol bonded to the iron atom in iron oxide clusters. Hydrogen transfer reactions occur from one of the C–H bonds of the methyl group and the O–H bond of the hydroxyl group for all dehydrogenation and neutral water elimination reactions, based on DFT calculations. Two parallel reaction pathways, hydro-

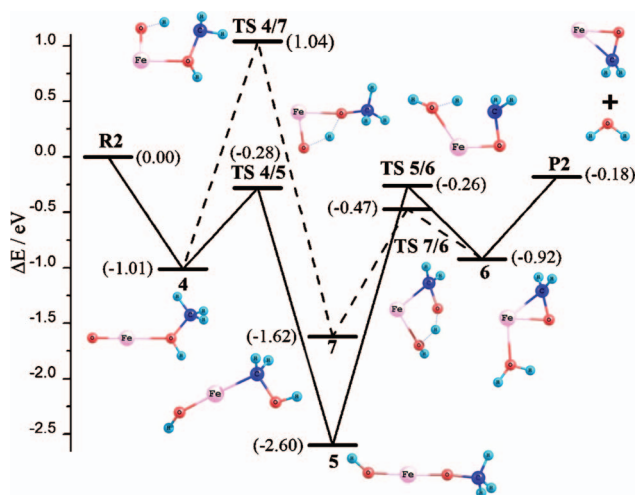


FIG. 4. (Color) Reaction pathways for  ${}^5\text{FeO}+\text{CH}_3\text{OH}\rightarrow(\text{CH}_2\text{O})^5\text{Fe}+\text{H}_2\text{O}$  calculated at the B3LYP/6-311+G(*d*) level. See caption of Fig. 3 for explanations. Energies are relative to the energy of the  ${}^5\text{FeO}+\text{CH}_3\text{OH}$  reactants. R2:  ${}^5\text{FeO}+\text{CH}_3\text{OH}$ ; P2:  $(\text{CH}_2\text{O})^5\text{Fe}+\text{H}_2\text{O}$ .

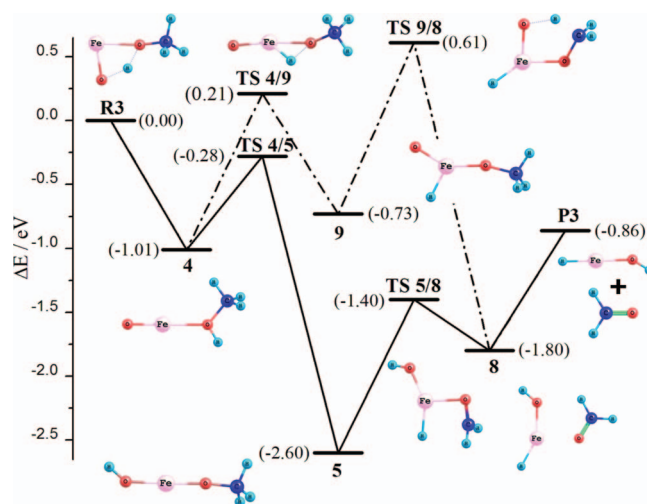


FIG. 5. (Color) Reaction pathways for  ${}^5\text{FeO}+\text{CH}_3\text{OH}\rightarrow\text{H}^5\text{FeOH}+\text{CH}_2\text{O}$  calculated at the B3LYP/6-311+G(*d*) level. See caption of Fig. 3 for explanations. Energies are relative to the energy of the  ${}^5\text{FeO}+\text{CH}_3\text{OH}$  reactants. The solid line indicates hydrogen transfer to the oxygen atom of FeO from the O–H group, and the dashed dot line indicates hydrogen transfer to the iron atom of FeO from the O–H group. R3:  ${}^5\text{FeO}+\text{CH}_3\text{OH}$ ; P3:  $\text{H}^5\text{FeOH}+\text{CH}_2\text{O}$ .

gen transfer from the O–H group followed by hydrogen transfer from the C–H group (pathway A), and the inverse process, hydrogen transfer from the C–H group followed by hydrogen transfer from the O–H group (pathway B), are both presented in Figs. 3–7.

An overall +0.09 eV reaction energy is determined for

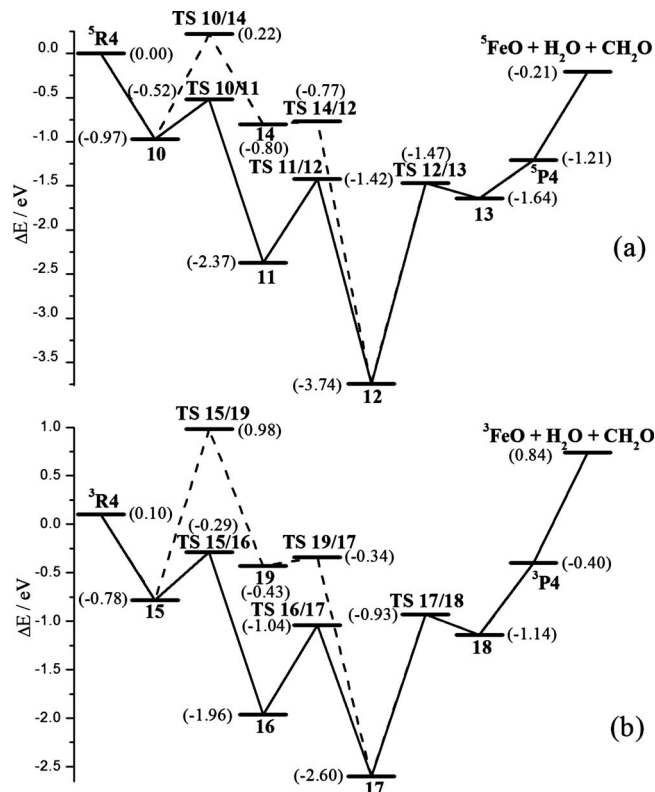


FIG. 6. Reaction pathways for (a)  ${}^5\text{FeO}_2$ , (b)  ${}^3\text{FeO}_2+\text{CH}_3\text{OH}\rightarrow(\text{H}_2\text{O})^{5/3}\text{FeO}+\text{CH}_2\text{O}$  calculated at the B3LYP/6-311+G(*d*) level. See caption of Fig. 3 for explanations. Energies are relative to the energy of the  ${}^5\text{FeO}_2+\text{CH}_3\text{OH}$  reactants. R4:  $\text{FeO}_2+\text{CH}_3\text{OH}$ ; P4:  $(\text{H}_2\text{O})\text{FeO}+\text{CH}_2\text{O}$ .

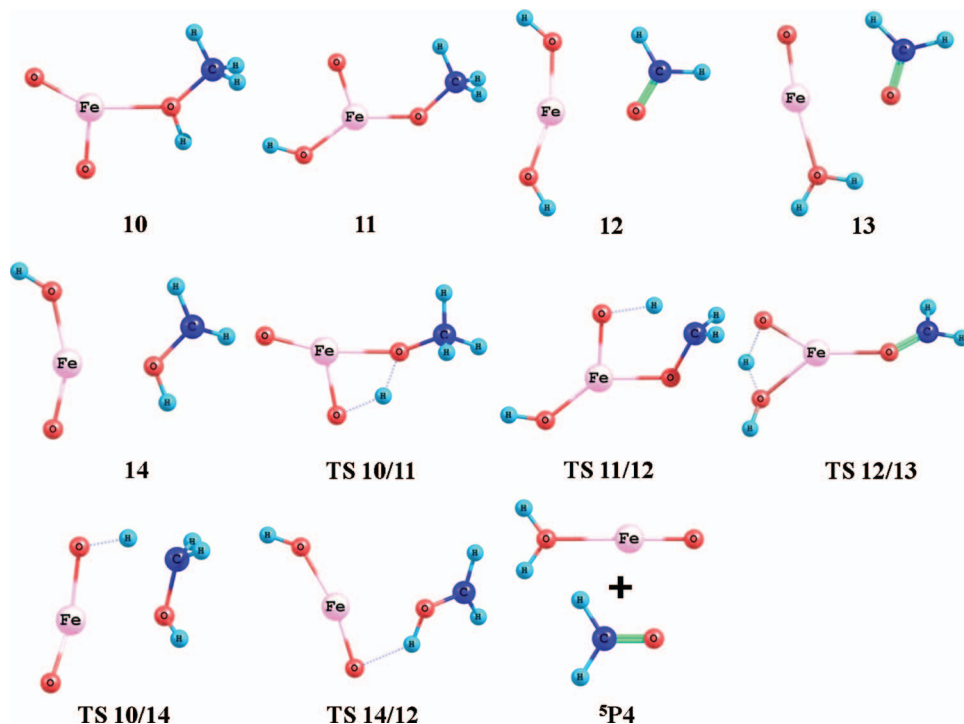


FIG. 7. (Color) Geometry parameters for the reactants, intermediates, transition states, and products involved in the reaction pathways presented in Fig. 6(a). Iron, oxygen, carbon, and hydrogen are in pink, red, dark blue, and light blue, respectively.

the methanol dehydrogenation reaction on an iron atom in its ground quintet state, and all four transition states, a three membered ring **TS 1/2** (0.48 eV), a four membered ring **TS 2/P1** (0.41 eV) from pathway A, a three membered ring **TS 1/3** (1.15 eV), and a three membered ring **TS 3/P1** (0.83 eV) from pathway B, are higher in energy than the initial structure  ${}^5\text{Fe} + \text{CH}_3\text{OH}$ , as shown in Fig. 3.

The quintet ground state for FeO has the lowest energy, and neutral water elimination and neutral formaldehyde elimination reactions are calculated to have  $-0.18$  and  $-0.86$  eV reaction energies, respectively. The exothermic reaction energies are consistent with the observation of the  $(\text{CH}_2\text{O})\text{Fe}$  and  $\text{HFeOH}$  products, as presented in Fig. 2(a). In addition, the O–H bond activation (pathway A, solid line in Fig. 4) is much more favorable than the C–H bond activation (pathway B, dashed line in Fig. 4), as **TS 4/5** ( $-0.28$  eV) versus **TS 4/7** (1.04 eV) in Fig. 4.  $\text{H}_2\text{O}$  is generated from the reaction with methanol when the O atom of FeO is involved in the hydrogen transfer (**TS 5/6**, **TS 7/6** in Fig. 4), whereas formaldehyde elimination occurs when the Fe atom is the receptor for the hydrogen transfer (**TS 5/8**, **TS 4/9** in Fig. 5).

Although  ${}^5\text{FeO}_2$  is slightly lower in energy than  ${}^3\text{FeO}_2$  by 0.10 eV at the B3LYP/6-311+G(*d*) level of theory,  $\text{FeO}_2$  has a triplet ground state according to previous experimental and theoretical results.<sup>30,43</sup> Neutral formaldehyde elimination for reaction of methanol with both quintet and triplet  $\text{FeO}_2$  is energetically favorable, with the overall reaction energies of  $-1.21$  and  $-0.40$  eV for the quintet and triplet states, respectively. Thus, the calculational results are in good agreement with the experimental observation of  $(\text{H}_2\text{O})\text{FeO}$  product (Fig. 2 and Table I). Similarly, reaction barriers for O–H activation (pathway A, solid line in Fig. 6) are lower than those for the C–H activation (pathway B, dashed line in Fig. 6) for the reaction of  ${}^{5/3}\text{FeO}_2$  with methanol, as shown by **TS 10/11** ( $-0.52$  eV) versus **TS 10/14** (0.22 eV), **TS 11/12**

( $-1.42$  eV) versus **TS 14/12** ( $-0.77$  eV) in Fig. 6(a) and **TS 15/16** ( $-0.29$  eV) versus **TS 15/19** (0.98 eV), **TS 16/17** ( $-1.04$  eV) versus **TS 19/17** ( $-0.34$  eV) in Fig. 6(b). Both pathways A for triplet and quintet  $\text{FeO}_2$  are overall barrierless processes; however, pathways B have overall barriers of  $+0.88$  ( $0.98 - 0.10 = 0.88$  eV) and  $+0.22$  eV for triplet and quintet  $\text{FeO}_2$ , respectively. Formaldehyde elimination reactions for pathways A are through a four membered ring transition state (**TS 10/11** or **TS 15/16**), a five membered ring transition state (**TS 11/12** or **TS 16/17**), and a four membered ring transition state (**TS 12/13** or **TS 17/18**), as presented in Figs. 6 and 7.

## IV. DISCUSSION

Ionic and neutral clusters are both generated by laser ablation and reacted in the fast flow reactor. The ions (reactants and products) are all removed by an electric field after the reactor. The influences of ion-molecule reactions and charge transfer in the fast flow reactor have been discussed previously in detail;<sup>40(m)</sup> the conclusion is that the small amount of ionic clusters, compared to the abundant neutral clusters, and does not play a role for the neutral cluster distribution and reactions. Therefore, all the discussed issues below only involve neutral cluster chemistry.

### A. $\text{FeCH}_2\text{O}$ generation

Because neutral species cannot be isolated by electric and magnetic fields like charged particles can, all the reactants, intermediates, and products are mixed together in the mass spectra after ionization. Identifying specific reaction products with particular reactions, even with the aid of isotopic substitution experiments, such as  $\text{Fe}_m\text{O}_n\text{CH}_3\text{OH}$  versus

$\text{Fe}_m\text{O}_{n+2}$ , and  $\text{Fe}_m\text{O}_n\text{CD}_3\text{OH}$  versus  $\text{Fe}_m\text{O}_{n+2}\text{HD}$ , thus becomes a problem. Nevertheless, DFT calculations help clarify product origins and identifications.

In Fig. 2, the  $\text{FeCH}_2\text{O}$  mass peak is observed and two possible reaction channels,  $\text{Fe}+\text{CH}_3\text{OH}\rightarrow(\text{CH}_2\text{O})\text{Fe}+\text{H}_2$  [reaction (7)] and  $\text{FeO}+\text{CH}_3\text{OH}\rightarrow(\text{CH}_2\text{O})\text{Fe}+\text{H}_2\text{O}$  [reaction (8)], are suggested: these two reaction energies are calculated as 0.09 and  $-0.18$  eV, respectively. Taking into account DFT calculational uncertainties (about 0.2 eV), both reactions (7) and (8) are reasonable reactions in the fast flow reactor based on thermodynamic considerations. PESs for the reaction  ${}^5\text{Fe}+\text{CH}_3\text{OH}\rightarrow(\text{CH}_2\text{O}){}^5\text{Fe}+\text{H}_2$  presented in Fig. 3 clearly indicate that a high reaction barrier exists for methanol dehydrogenation by a quintet iron atom. Pathway A barriers are calculated as 0.48 eV for hydrogen transfer from the O–H group of methanol to the iron atom via a three membered ring transition state (TS 1/2), followed by a 0.41 eV for the other hydrogen transfer from the C–H group via a four membered ring transition state (TS 2/P1). For pathway B, hydrogen transfer from the C–H group followed by that from the O–H group, the related transition states are 1.15 (TS 1/3) and 0.83 eV (TS 3/P1) higher in energy than the initial structure,  ${}^5\text{Fe}+\text{CH}_3\text{OH}$ . All four reaction barriers for pathways A and B are much higher than the initial energy. Therefore the reaction  ${}^5\text{Fe}+\text{CH}_3\text{OH}\rightarrow(\text{CH}_2\text{O}){}^5\text{Fe}+\text{H}_2$  is dynamically unfavorable in our experiments according to the PES calculations.

On the other hand, the neutral water elimination reaction  ${}^5\text{FeO}+\text{CH}_3\text{OH}\rightarrow(\text{CH}_2\text{O}){}^5\text{Fe}+\text{H}_2\text{O}$  has relatively low reaction barriers as shown in Fig. 4. In particular, for pathway A, transition state TS 4/5 at  $-0.28$  eV in energy is obtained via a four membered ring, followed by a five membered ring transition state TS 5/6 ( $-0.26$  eV). For pathway B, the transition states are calculated as 1.04 eV for TS 4/7 via a five membered ring and  $-0.47$  eV for TS 7/6 via a four membered ring, respectively. The low reaction barriers for pathway A ( $-0.28$  and  $-0.26$  eV) indicate that the reaction of  ${}^5\text{FeO}+\text{CH}_3\text{OH}\rightarrow(\text{CH}_2\text{O}){}^5\text{Fe}+\text{H}_2\text{O}$  is an overall barrierless process and an exothermic reaction. The high barrier (1.04 eV) for pathway B suggests that hydrogen from the C–H group of methanol cannot migrate to FeO before hydrogen transfer from the O–H group occurs. Pathway A is more favorable than pathway B probably because the calculated bond strength of  $\text{HOFe}-\text{OCH}_3$  (1.74 eV) is larger than that of  $\text{HOFe}-\text{OHCH}_2$  (1.67 eV). The PES calculations shown in Figs. 3 and 4 suggest that reaction product  $(\text{CH}_2\text{O})\text{Fe}$  comes from the water elimination reaction of the neutral FeO cluster with methanol [reaction (8)], instead of a dehydrogenation reaction of a neutral Fe atom with methanol [reaction (7)], and in particular, hydrogen transfer from the O–H group of methanol occurs prior to that from the C–H group of methanol.

## B. Neutral formaldehyde elimination reactions

Observation of  $\text{Fe}_m\text{O}_n\text{H}_2$  ( $m=1-2$ ,  $n=1-5$ ) in Fig. 2 and Table I suggest that the neutral formaldehyde elimination reactions,  $\text{Fe}_m\text{O}_n+\text{CH}_3\text{OH}\rightarrow\text{Fe}_m\text{O}_n\text{H}_2+\text{CH}_2\text{O}$ , occur in the fast flow reactor. Additionally, deuterated methanol experi-

ments indicate that the hydrogens of  $\text{Fe}_m\text{O}_n\text{H}_2$  come from both the O–H and C–H groups of methanol. The PESs for reactions  ${}^5\text{FeO}+\text{CH}_3\text{OH}\rightarrow\text{H}{}^5\text{FeOH}+\text{CH}_2\text{O}$ ,  ${}^{5/3}\text{FeO}_2+\text{CH}_3\text{OH}\rightarrow(\text{H}_2\text{O})^{5/3}\text{FeO}+\text{CH}_2\text{O}$  are calculated by DFT and presented in Figs. 5–7. Similar to the water elimination reaction on FeO as shown in Fig. 4, pathway A, for neutral formaldehyde elimination on  $\text{FeO}_2$ , is energetically favorable, whereas pathway B, is thermodynamically unfavorable, for neutral formaldehyde elimination reactions.

For reaction  ${}^5\text{FeO}+\text{CH}_3\text{OH}\rightarrow\text{H}{}^5\text{FeOH}+\text{CH}_2\text{O}$ , no pathway B is involved. Hydrogen transfers from the O–H group of methanol to either the O atom or the Fe atom of the FeO, as shown in Fig. 5. In addition, the pathway for hydrogen transfer from the O–H group to the Fe atom has high reaction barriers, 0.21 eV for TS 4/9 and 0.61 eV for TS 9/8, whereas hydrogen transfer to the O atom of FeO has low reaction barriers,  $-0.28$  eV for TS 4/5 and  $-1.40$  eV for TS 5/8.

One may argue that the reaction intermediates 12 or 17 in Figs. 6 and 7 can dissociate directly to form  $\text{Fe}(\text{OH})_2+\text{CH}_2\text{O}$  in the reaction  $\text{FeO}_2+\text{CH}_3\text{OH}\rightarrow(\text{H}_2\text{O})\text{FeO}+\text{CH}_2\text{O}$ ; however, the structure  $\text{Fe}(\text{OH})_2$  is calculated to be an unstable conformer: it does not converge to a stable structure at the B3LYP/6-311+G(*d*) level. Only conformers  $(\text{H}_2\text{O})\text{FeO}$  and  $(\text{HO})(\text{H})\text{FeO}$  are stable structures at this theory level, as presented in Figs. 8(a) and 8(b). The conformer  $(\text{H}_2\text{O}){}^5\text{FeO}$  is lower in energy than the conformer  $(\text{HO})(\text{H}){}^5\text{FeO}$  by 0.38 eV. Thus, the product structure is  $(\text{H}_2\text{O})\text{FeO}$ , no matter which intermediate, 12 or 17 dissociates. Calculations at the MP2/6-311+G(*d*) level show that the structure  $\text{Fe}(\text{OH})_2$  is a stable structure; however, it is not the lowest energy conformer.

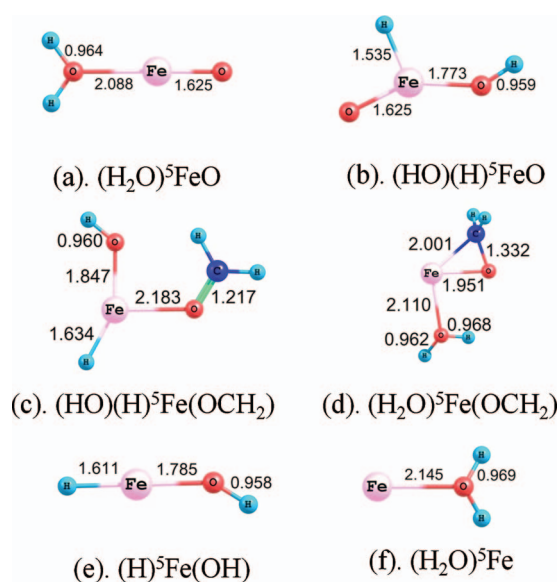
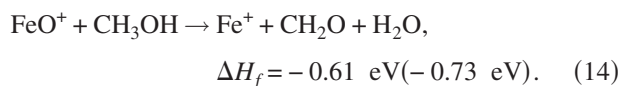
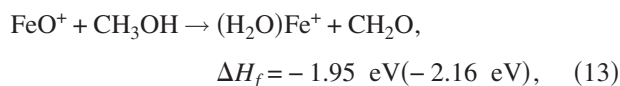
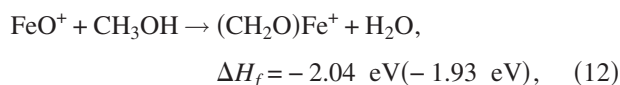
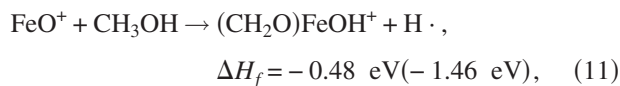


FIG. 8. (Color) Geometry parameters for reaction intermediates (a).  $(\text{H}_2\text{O}){}^5\text{FeO}$ ; (b).  $(\text{HO})(\text{H}){}^5\text{FeO}$ ; (c).  $(\text{HO})(\text{H}){}^5\text{Fe}(\text{OCH}_2)$ ; (d).  $(\text{H}_2\text{O}){}^5\text{Fe}(\text{OCH}_2)$ ; (e).  $(\text{H}){}^5\text{Fe}(\text{OH})$ ; and (f).  $(\text{H}_2\text{O}){}^5\text{Fe}$ . Iron, oxygen, carbon, and hydrogen are in pink, red, dark blue, and light blue, respectively. See text for detail.

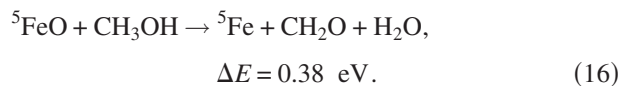
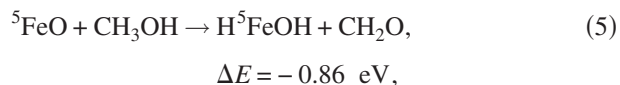
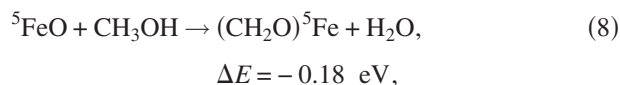
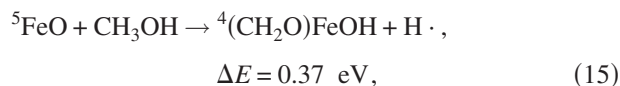
### C. Comparisons with studies for ion-molecule reactions

Reaction of charged  $\text{Fe}_m\text{O}_n$  clusters with methanol has been investigated experimentally<sup>12(d),16,19</sup> and theoretically.<sup>15(a)</sup> Comparison of the reactions of neutral and ionic clusters, including product identification and structures, reaction pathways, and reaction mechanisms, can help us understand the effect of charge on condensed phase surface catalytic reactions.

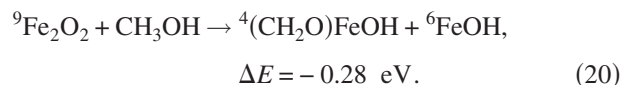
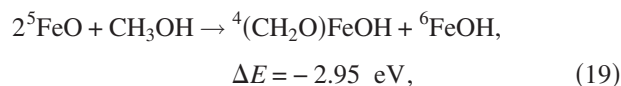
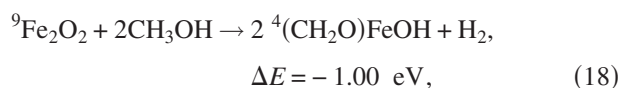
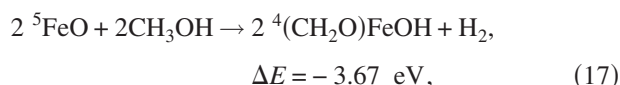
Four types of ion reactions are identified by FTICRMS for the overall reaction of  $\text{FeO}^+$  with methanol.<sup>12(d)</sup> All four reactions are exothermic based on thermochemical data considerations<sup>12(d)</sup> and DFT calculational results.<sup>15(a)</sup> (DFT calculational results for sextet  $\text{FeO}^+$  are presented in parenthesis)



The related neutral cluster reaction energies are calculated by DFT as



Hydrogen radical generation is favorable for the cationic cluster reaction (11), but unfavorable for the neutral cluster reaction (15). Observation of product  $(\text{CH}_2\text{O})\text{FeOH}$  in Fig. 2 suggests that the reaction mechanism perhaps involves multiple molecule collisions, such as



Reactions (19) and (20) are more likely to occur in the reactor, because products  $(\text{CH}_2\text{O})\text{FeOH}$  and  $\text{FeOH}$ , are both observed in Fig. 2. Similarly, observation of  $\text{Fe}_2\text{O}_2\text{H}$  (Fig. 2 and Table I) can also be understood in the same manner as above for  $\text{FeOH}$ .

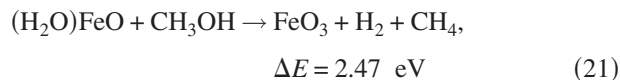
For reaction (5), an intermediate structure (8)  $(\text{HO})-(\text{H})\text{Fe}(\text{OCH}_2)$  is obtained and shown in Fig. 5. As presented in Figs. 8(c)–8(f), the neutral structure  $(\text{HO})-(\text{H})\text{Fe}(\text{OCH}_2)$  is more stable than its conformer structure  $(\text{H}_2\text{O})\text{Fe}(\text{OCH}_2)$  by 0.90 eV, and the following dissociation product,  $(\text{H})\text{Fe}(\text{OH})$ , for which both hydrogen and the hydroxyl group are bonded to the Fe atom, is also more stable than  $(\text{H}_2\text{O})\text{Fe}$  by 0.81 eV. As a comparison,  $(\text{H}_2\text{O})\text{Fe}^+(\text{OCH}_2)$  is the most stable structure and  $(\text{H}_2\text{O})\text{Fe}^+$  is the most stable dissociation product for the related cationic reaction (12).<sup>15(a)</sup> Thus, even though the product mass numbers are the same for the reactions of  $\text{FeO}$  or  $\text{FeO}^+$  with methanol, the product structures and reaction pathways are significantly different based on DFT calculations.

Reaction (16) cannot be solely identified in our neutral cluster studies, since the signal of the product Fe atom overlaps with that of the reactant Fe atom. Even though an increase of the Fe signal is observed after reaction of  $\text{Fe}_m\text{O}_n$  neutral clusters with methanol, as seen in Fig. 2, reaction (16) is thermodynamically unfavorable based on the DFT calculations. The reasons for the observation of the increasing Fe signal in Fig. 2 are not completely understood, but probably involve multiple collisions and reactions. A neutral cluster must be ionized to be detected, and the cross sections associated with each cluster can be different, and difficult to estimate. Therefore, the relatively large increase in the Fe product signal may correspond to its high cross section, whereas the related reactant signal decreases can be too small to be observed because of the low ionization cross sections associated with their particular species. Thus, the Fe signal can be generated by many different reaction sources, and the decrease/increase in product and reactant signals do not directly correlate with relative species concentrations.

Pathway A (hydrogen transfer from the O–H group followed by that from the C–H group) and pathway B (hydrogen transfer from the C–H group followed by that from the O–H group) have also been calculated for the reaction of  $\text{FeO}^+$  with methanol.<sup>15(a)</sup> Both pathways are energetically favorable and the reaction barriers are close, which indicates that these two pathways are competitive for cationic  $\text{FeO}^+$  reactions. Only pathway A is thermodynamically favorable for the neutral cluster reactions, however.

Reactions of anionic  $\text{FeO}_2^-$ ,  $\text{Fe}_2\text{O}_3^-$ , and  $\text{Fe}_2\text{O}_4^-$  with methanol and deuterated methanol have also been investigated.<sup>19</sup> Observations of  $\text{FeO}_2\text{HD}^-$  by employing deuterated methanol,  $\text{CH}_3\text{OD}$ , and  $\text{CD}_3\text{OH}$ , indicate that the hydrogens of  $\text{FeO}_2\text{H}_2^-$  are from both O–H and C–H groups;

this is consistent with our results for the neutral cluster studies. The structure of  $\text{FeO}_2\text{H}_2^-$  is suggested as  $\text{Fe}(\text{OH})_2^-$ , however, with two hydroxyl groups bonded to the Fe atom, whereas the most stable structure for neutral species is calculated as  $(\text{H}_2\text{O})\text{FeO}$ , as shown in Fig. 8(a), suggesting a different reaction mechanism for anionic and neutral cluster reactions. Secondary reaction products for  $\text{Fe}(\text{OH})_2^-$  have also been obtained, which imply the reaction  $\text{FeO}_2\text{H}_2^- + \text{CH}_3\text{OH} \rightarrow \text{FeO}_3^- + \text{H}_2 + \text{CH}_4$  occurs; however, the reaction energy for related neutral  $(\text{H}_2\text{O})\text{FeO}$  cluster reaction is calculated as 2.47 eV. This high reaction energy clearly indicates that the secondary reaction,



does not occur in the fast flow reactor.

Oxidation of methanol to formaldehyde by  $\text{FeO}^{2+}$  in the gas phase and in the solution has been calculated by DFT.<sup>16</sup> Interestingly, Pathway B, hydrogen transfer from the C–H group of methanol followed by that from the O–H group, is given as the most likely mechanism. In addition, the product structure,  $(\text{H}_2\text{O})\text{Fe}^{2+}$ , which is similar to  $(\text{H}_2\text{O})\text{Fe}^+$  with a water molecule bonded to the Fe atom through the O atom, is different from related neutral species,  $\text{HFeOH}$ , as shown in Fig. 8(e).

The product distribution for cationic [reactions (11)–(14)]  $\text{FeO}^+$  and neutral  $\text{FeO}$  cluster reactions (Fig. 2 and Table I) with methanol are different:  $\text{FeOH}$ ,  $(\text{CH}_2\text{O})\text{FeOH}$ , and association product  $\text{Fe}_m\text{O}_n\text{CH}_3\text{OH}$ , are observed only for the neutral clusters reactions, and are not present for the cationic reactions. These differences clearly indicate that neutral cluster chemistry, rather than ion cluster chemistry, occurs in the fast flow reactor. As pointed out at the beginning of this discussion and in the literature [Ref. 40(m)], the neutral cluster contribution in a laser ablated sample is much larger than that of the ionic clusters. Therefore, the observed product distribution (see Fig. 2 and Table I) arises from neutral  $\text{Fe}_m\text{O}_n$  cluster chemistry and not from ion cluster chemistry.

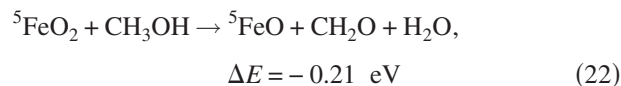
#### D. Comparison with other transition metal oxides

Dehydrogenation reactions are also observed as a dominant reaction for cationic  $\text{VO}^+$  and neutral  $\text{VO}$  clusters,  $\text{VO}^{0/+} + \text{CH}_3\text{OH} \rightarrow (\text{CH}_2\text{O})\text{VO}^{0/+} + \text{H}_2$ ,<sup>12(a),40(n)</sup> however, as a comparison, neutral water elimination, and association are primary reactions for the neutral  $\text{FeO}$  cluster, and no dehydrogenation products are detected (see Fig. 2 and Table I). The dissociation energies for  $\text{VO}$  and  $\text{FeO}$  are estimated as  $D^\circ(\text{V}-\text{O}) = 625.5 \pm 8.5 \text{ kJ/mol}$  (Ref. 44) and  $D^\circ(\text{Fe}-\text{O}) = 389.1 \pm 12.6 \text{ kJ/mol}$ ,<sup>45</sup> therefore the Fe–O bond is more readily cleaved than the V–O bond. As a result, the neutral water elimination reaction is more favorable for  $\text{FeO} + \text{CH}_3\text{OH}$ , whereas the dehydrogenation reaction is more favorable for  $\text{VO} + \text{CH}_3\text{OH}$ . Only Pathway B, hydrogen transfer from the C–H group followed by that from the O–H group, is energetically favorable for reaction of  $\text{VO}^+$  with methanol, and pathway A does not occur for this reaction. For  $\text{VO}_2^{0/+}$ , two reaction channels, neutral water elimination

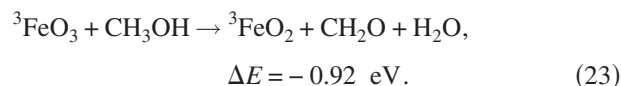
and formaldehyde elimination, are identified and  $\text{CH}_2\text{O}$  elimination is the primary reaction pathway (72%) for the cationic reaction. Nevertheless, only the neutral formaldehyde elimination reaction is observed for the reaction of  $\text{FeO}_2$  with methanol.

#### E. Understanding of the condensed phase methanol oxidation to formaldehyde at a molecular level

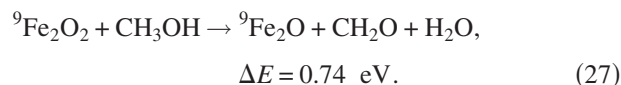
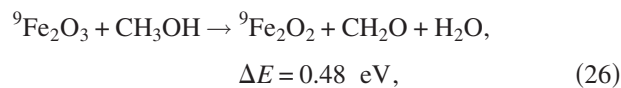
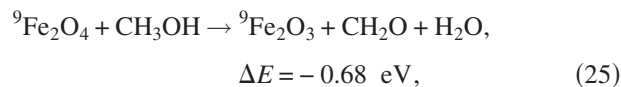
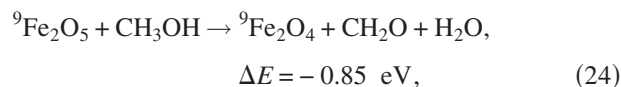
The bond length of  $\text{H}_2\text{O}-^5\text{FeO}$  in Fig. 8(a) is calculated as 2.088 Å: it is much longer than a typical Fe–O bond in  $\text{FeO}_2$  (1.606 Å for  $^5\text{FeO}_2$ ). Thus, the water molecule is weakly bound in  $\text{H}_2\text{O}-^5\text{FeO}$  and can be readily dissociated from  $(\text{H}_2\text{O})\text{FeO}$  to form  $\text{FeO} + \text{H}_2\text{O}$ . Subsequently, the calculated reaction energy for the reaction of  $^5\text{FeO}_2$  with methanol indicates that this reaction is exothermic,



and for  $\text{FeO}_3$ , the reaction is



Additionally, according to previous calculational results,<sup>40(a)</sup> the ground states for  $\text{Fe}_2\text{O}_n$  ( $n=1, 2, 3$ , and 5) clusters are nonets, and the ground state for  $\text{Fe}_2\text{O}_4$  is a septet. The energy difference for  $^7\text{Fe}_2\text{O}_4$  and  $^9\text{Fe}_2\text{O}_4$  is only 0.02 eV, however. Thus, reaction energies for  $^9\text{Fe}_2\text{O}_n + \text{CH}_3\text{OH} \rightarrow ^9\text{Fe}_2\text{O}_n\text{H}_2 + \text{CH}_2\text{O} \rightarrow ^9\text{Fe}_2\text{O}_{n-1} + \text{CH}_2\text{O} + \text{H}_2\text{O}$  are calculated at the B3LYP/6-311+G(d) level as



Obviously, methanol oxidation reactions only occur on oxygen rich clusters, such as  $\text{FeO}_2$ ,  $\text{FeO}_3$ ,  $\text{Fe}_2\text{O}_4$ , and  $\text{Fe}_2\text{O}_5$ . Reaction pathways for reactions (23)–(25) are also calculated and presented in the Supporting Information. Note only pathway A is considered for these calculations. The reaction energies and overall reaction energy barriers for reactions (22), (23), and (25) are calculated as  $-0.21/-0.52$ ,  $-0.92/-0.16$ , and  $-0.68/-0.29 \text{ eV}$ , respectively. The potential energy surfaces for reactions (23) and (25) are presented in the Supporting Information Figs. S1 and S2.<sup>46</sup> The  $\text{Fe}_2\text{O}_5$  cluster has two conformers: conformer A, the lowest energy conformer, is the structure that an oxygen molecule bound to the iron atom; and conformer B, the structure for which the two oxygen atoms are separated. Conformer B is higher in energy

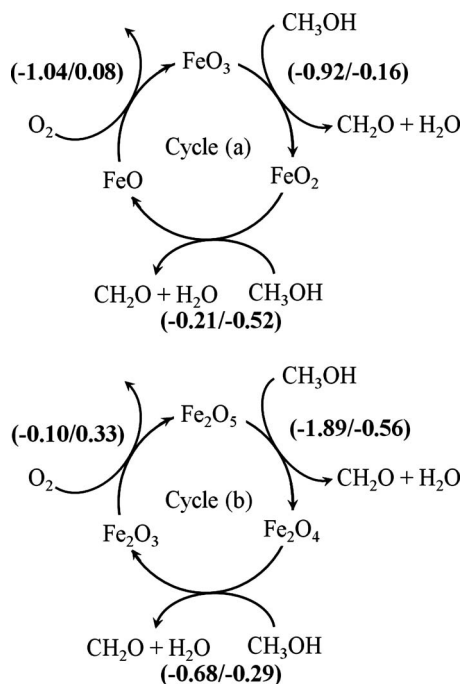


FIG. 9. Proposed catalysis cycles for the reaction  $\text{CH}_3\text{OH} + 1/2 \text{O}_2 \rightarrow \text{CH}_2\text{O} + \text{H}_2\text{O}$  over (a)  $\text{FeO}_3/\text{FeO}_2/\text{FeO}$  and (b)  $\text{Fe}_2\text{O}_5/\text{Fe}_2\text{O}_4/\text{Fe}_2\text{O}_3$  clusters. Reaction energies (a) and overall barriers (b) are listed for each reaction as (A/B) in eV.

than conformer A by 1.04 eV. Potential energy surfaces for reaction (24) for both conformers B and A are calculated and presented in the Supporting Information Figs. S3 and S4;<sup>46</sup> the reaction energies and overall reaction energy barriers are calculated as  $-1.89/-0.56$  and  $-0.85/0.53$  eV, respectively. Apparently reactions (23), (24) (for conformer B), and (25) are thermodynamically favorable and overall barrierless processes.

The oxidation processes,  $5\text{FeO} + \text{O}_2 \rightarrow 5\text{FeO}_3$  and  $9\text{Fe}_2\text{O}_3 + \text{O}_2 \rightarrow 9\text{Fe}_2\text{O}_5$ , have been investigated computationally.<sup>40(a)</sup> The reaction energies and overall reaction energy barriers are estimated as  $-1.04/0.08$  eV for FeO oxidation to FeO<sub>3</sub> and  $-0.10/0.33$  eV for Fe<sub>2</sub>O<sub>3</sub> oxidation to Fe<sub>2</sub>O<sub>5</sub> conformer B, respectively.<sup>40(a)</sup> Thus, the condensed phase catalytic cycles can be suggested and are presented in Fig. 9. FeO<sub>3</sub> and FeO<sub>2</sub> can be reduced to FeO<sub>2</sub> and FeO, respectively, by CH<sub>3</sub>OH to form CH<sub>2</sub>O + H<sub>2</sub>O, and the generated FeO is subsequently oxidized by O<sub>2</sub> and FeO<sub>3</sub> is regenerated (cycle a). Similar to the FeO<sub>3</sub>/FeO<sub>2</sub>/FeO cycle, methanol can be oxidized by Fe<sub>2</sub>O<sub>5</sub> and Fe<sub>2</sub>O<sub>4</sub> clusters, and the generated Fe<sub>2</sub>O<sub>3</sub> can be oxidized to Fe<sub>2</sub>O<sub>5</sub> by O<sub>2</sub> (cycle b). Oxygen dissociation on the FeO and Fe<sub>2</sub>O<sub>3</sub> surfaces is the rate limiting step for these two catalysis cycles, similar to the conclusions for the reaction of Fe<sub>m</sub>O<sub>n</sub> with CO.<sup>40(a)</sup>

An isotopic <sup>18</sup>O<sub>2</sub> experiment can prove the above proposed catalytic cycles. If H<sub>2</sub><sup>18</sup>O is observed after reaction of methanol on Fe<sub>m</sub><sup>18</sup>O<sub>n</sub> (Fe<sub>m</sub>O<sub>n</sub> = FeO<sub>2</sub>, FeO<sub>3</sub>, Fe<sub>2</sub>O<sub>4</sub>, and Fe<sub>2</sub>O<sub>5</sub>) clusters, one can conclude that the Fe–O bond is broken in the reaction, and <sup>18</sup>O transfers from iron oxide to form H<sub>2</sub>O, as presented in reactions (22)–(25).

## V. CONCLUSIONS

Reactions of neutral iron oxide clusters with methanol are studied by time of flight mass spectrometry employing

118 nm SPI and DFT calculations. Direct association reaction is observed for the FeO cluster, and methanol dehydrogenation reactions are detected for FeO<sub>1,2</sub> and Fe<sub>2</sub>O<sub>2–5</sub> clusters. DFT calculations are additionally performed and the following conclusions can be drawn from the theoretical studies: (1) the O–H bond of methanol is more readily activated by iron oxide than the C–H bond of the methyl group, and hydrogen transfer from the O–H group occurs prior to that from the C–H group; (2) neutral water elimination reactions are energetically more favorable than dehydrogenation reactions on iron oxide clusters; (3) for the product FeCH<sub>2</sub>O, the reaction of iron monoxide with methanol ( $\text{FeO} + \text{CH}_3\text{OH} \rightarrow \text{FeCH}_2\text{O} + \text{H}_2\text{O}$ ) is an overall barrierless process, whereas the reaction of iron atom with methanol ( $\text{Fe} + \text{CH}_3\text{OH} \rightarrow \text{FeCH}_2\text{O} + \text{H}_2$ ) has high reaction barriers (0.41–1.15 eV); (4) neutral formaldehyde (CH<sub>2</sub>O) is suggested to be generated from the reactions of FeO<sub>1,2</sub> and Fe<sub>2</sub>O<sub>2–5</sub> with CH<sub>3</sub>OH at room temperature based on experimental observations. The various reaction mechanisms explored by DFT are in good agreement with the experimental results, and the condensed phase methanol oxidation to formaldehyde catalytic reaction can be understood by the proposed cluster catalytic cycles.

## ACKNOWLEDGMENTS

This work was supported by the U.S. DOE BES program, ASFOR, the NSFERC for Extreme Ultraviolet Science and Technology under NSF Award No. 0310717, and the National Center for Supercomputing Applications under Grant No. CHE080018N.

- <sup>1</sup>J. L. G. Fierro, *Metal Oxides Chemistry and Applications* (Taylor & Francis, London, 2006).
- <sup>2</sup>G. Ertl, H. Knözinger, and J. Weitkamp, *Handbook of Heterogeneous Catalysis* (Wiley-VCH, Weinheim, 1997).
- <sup>3</sup>D. K. Böhme and H. Schwarz, *Angew. Chem., Int. Ed.* **44**, 2336 (2005).
- <sup>4</sup>J. R. Wilson and G. Burgh, *Energizing our Future: Rational Choices for the 21st Century* (Wiley, Hoboken, NJ, 2008).
- <sup>5</sup>G. A. Olah, A. Goepfert, and G. K. S. Prakash, *Beyond Oil and Gas: the Methanol Economy* (Wiley-VCH, Weinheim, 2006).
- <sup>6</sup>G. C. Chinchin, P. J. Denny, J. R. Jennings, M. S. Spencer, and K. C. Waugh, *Appl. Catal.* **36**, 1 (1988).
- <sup>7</sup>X. M. Liu, G. Q. Lu, Z. F. Yan, and J. Beltramini, *Ind. Eng. Chem. Res.* **42**, 6518 (2003).
- <sup>8</sup>A. P. V. Soares, M. F. Portela, and A. Kiennemann, *Catal. Rev. - Sci. Eng.* **47**, 125 (2005).
- <sup>9</sup>M. P. House, A. F. Carley, and M. Bowker, *J. Catal.* **252**, 88 (2007).
- <sup>10</sup>C. T. Wang and R. J. Willey, *J. Catal.* **202**, 211 (2001).
- <sup>11</sup><http://webbook.nist.gov/chemistry>.
- <sup>12</sup>(a) M. Engeser, D. Schröder, and H. Schwarz, *Chem.-Eur. J.* **11**, 5975 (2005); (b) M. Engeser, D. Schröder, and H. Schwarz, *Eur. J. Inorg. Chem.* **17**, 2454 (2007); (c) S. Feysel, L. Scharfenberg, C. Daniel, H. Hartl, D. Schröder, and H. Schwarz, *J. Phys. Chem. A* **111**, 3278 (2007); (d) D. Schröder, R. Wesendrup, C. A. Schalley, W. Zummack, and H. Schwarz, *Helv. Chim. Acta* **79**, 123 (1996); (e) D. Schröder and H. Schwarz, *Angew. Chem., Int. Ed. Engl.* **29**, 1433 (1990); (f) D. Schroeder, A. Fiedler, J. Hrušák, and H. Schwarz, *J. Am. Chem. Soc.* **114**, 1215 (1992); (g) D. Schröder and H. Schwarz, *Helv. Chim. Acta* **75**, 1281 (1992); (h) H. Becker, D. Schröder, W. Zummack, and H. Schwarz, *J. Am. Chem. Soc.* **116**, 1096 (1994); (i) D. Schröder, H. Schwarz, D. E. Clemmer, Y. Chen, P. B. Armentrout, V. I. Baranov, and D. K. Böhme, *Int. J. Mass Spectrom. Ion Process.* **161**, 175 (1997); (j) S. Bärsch, D. Schröder, and H. Schwarz, *Helv. Chim. Acta* **83**, 827 (2000); (k) D. Schröder, P. Jackson, and H. Schwarz, *Eur. J. Inorg. Chem.* **6**, 1171 (2000); (l) P. Jackson, J. N. Harvey, D. Schröder, and H. Schwarz, *Int. J. Mass. Spectrom.* **204**, 233 (2001); (m) D. Schröder and H. Schwarz, *ibid.*

- 227, 121 (2003).
- <sup>13</sup> (a) D. R. Justes, N. A. Moore, and A. W. Castleman, Jr., *J. Phys. Chem. B* **108**, 3855 (2004); (b) N. M. Reilly, J. U. Reveles, G. E. Johnson, S. N. Khanna, and A. W. Castleman, Jr., *Chem. Phys. Lett.* **435**, 295 (2007); (c) N. M. Reilly, J. U. Reveles, G. E. Johnson, S. N. Khanna, and A. W. Castleman, Jr., *J. Phys. Chem. A* **111**, 4158 (2007); (d) N. M. Reilly, J. U. Reveles, G. E. Johnson, J. M. Campo, S. N. Khanna, A. M. Köster, and A. W. Castleman, Jr., *J. Phys. Chem. C* **111**, 19086 (2007).
- <sup>14</sup> E. F. Fialko, A. V. Kikhtenko, and V. B. Goncharov, *Organometallics* **17**, 25 (1998).
- <sup>15</sup> (a) K. Yoshizawa and Y. Kagawa, *J. Phys. Chem. A* **104**, 9347 (2000); (b) K. Yoshizawa, Y. Shiota, Y. Kagawa, and T. Yamabe, *ibid.* **104**, 2552 (2000).
- <sup>16</sup> M. J. Louwse, P. Vassilev, and E. J. Baerends, *J. Phys. Chem. A* **112**, 1000 (2008).
- <sup>17</sup> (a) Y. Cao, X. Zhao, B. Xin, S. Xiong, and Z. Tang, *J. Mol. Struct.: THEOCHEM* **683**, 141 (2004); (b) **724**, 229 (2005).
- <sup>18</sup> P. Jackson, K. J. Fisher, and G. D. Willett, *Chem. Phys.* **262**, 179 (2000).
- <sup>19</sup> M. C. Oliveira, J. Marcalo, M. C. Vieira, and M. A. A. Ferreira, *Int. J. Mass. Spectrom.* **185–187**, 825 (1999).
- <sup>20</sup> J. Döbler, M. Pritzsche, and J. Sauer, *J. Am. Chem. Soc.* **127**, 10861 (2005).
- <sup>21</sup> P. Boulet, A. Baiker, H. Chermette, F. Gilardoni, J. C. Volta, and J. Weber, *J. Phys. Chem. B* **106**, 9659 (2002).
- <sup>22</sup> A. Goodrow and A. T. Bell, *J. Phys. Chem. C* **112**, 13204 (2008).
- <sup>23</sup> (a) B. V. Reddy, F. Rasouli, M. R. Hajaligol, and S. N. Khanna, *Chem. Phys. Lett.* **384**, 242 (2004); (b) B. V. Reddy and S. N. Khanna, *Phys. Rev. Lett.* **93**, 068301 (2004).
- <sup>24</sup> T. Feng and J. M. Vohs, *J. Phys. Chem. B* **109**, 2120 (2005).
- <sup>25</sup> T. Kim and I. E. Wachs, *J. Catal.* **255**, 197 (2008).
- <sup>26</sup> J. R. Jennings, *Catalytic Ammonia Synthesis: Fundamentals and Practice* (Plenum, New York, 1991).
- <sup>27</sup> D. S. Newsome, *Catal. Rev. - Sci. Eng.* **21**, 275 (1980).
- <sup>28</sup> C. Rhodes, G. J. Hutchings, and A. M. Ward, *Catal. Today* **23**, 43 (1995).
- <sup>29</sup> (a) H. Wu, S. R. Desai, and L.-S. Wang, *J. Am. Chem. Soc.* **118**, 5296 (1996); (b) L.-S. Wang, H. Wu, and S. R. Desai, *Phys. Rev. Lett.* **76**, 4853 (1996); (c) G. L. Gutsev, C. W. Bauschlicher, H. J. Zhai, and L.-S. Wang, *J. Chem. Phys.* **119**, 11135 (2003).
- <sup>30</sup> G. L. Gutsev, S. N. Khanna, B. K. Rao, and P. Jena, *J. Phys. Chem. A* **103**, 5812 (1999).
- <sup>31</sup> R. B. Metz, C. Nicolas, M. Ahmed, and S. R. Leone, *J. Chem. Phys.* **123**, 114313 (2005).
- <sup>32</sup> (a) H. Shiroishi, T. Oda, I. Hamada, and N. Fujima, *Polyhedron* **24**, 2472 (2005); (b) H. Shiroishi, T. Oda, I. Hamada, and N. Fujima, *Eur. Phys. J. D* **24**, 85 (2003).
- <sup>33</sup> Z. Cao, M. Duran, and M. Solà, *Chem. Phys. Lett.* **274**, 411 (1997).
- <sup>34</sup> A. T. García-sosa and M. Castro, *Int. J. Quantum Chem.* **80**, 307 (2000).
- <sup>35</sup> (a) M. Sakurai, K. Sumiyama, Q. Sun, and Y. Kawazoe, *J. Phys. Soc. Jpn.* **68**, 3497 (1999); (b) Q. Wang, Q. Sun, M. Sakurai, J. Z. Yu, B. L. Gu, K. Sumiyama, and Y. Kawazoe, *Phys. Rev. B* **59**, 12672 (1999); (c) Q. Sun, M. Sakurai, Q. Wang, J. Z. Yu, G. H. Wang, K. Sumiyama, and Y. Kawazoe, *ibid.* **62**, 8500 (2000).
- <sup>36</sup> M. M. Kappes and R. H. Staley, *J. Am. Chem. Soc.* **103**, 1286 (1981).
- <sup>37</sup> D. M. Huang, D. B. Cao, Y. W. Li, and H. Jiao, *J. Phys. Chem. B* **110**, 13920 (2006).
- <sup>38</sup> I. Zilberberg, M. Ilchenko, O. Isayev, L. Gorb, and J. Leszczynski, *J. Phys. Chem. A* **108**, 4878 (2004).
- <sup>39</sup> (a) J. M. C. Plane and R. J. Rollason, *Phys. Chem. Chem. Phys.* **1**, 1843 (1999); (b) R. J. Rollason and J. M. C. Plane, *ibid.* **2**, 2335 (2000).
- <sup>40</sup> (a) W. Xue, Z. C. Wang, S. G. He, Y. Xie, and E. R. Bernstein, *J. Am. Chem. Soc.* **130**, 15879 (2008); (b) D. N. Shin, Y. Matsuda, and E. R. Bernstein, *J. Chem. Phys.* **120**, 4157 (2004); (c) Y. Matsuda, D. N. Shin, and E. R. Bernstein, *ibid.* **120**, 4165 (2004); (d) Y. Matsuda, D. N. Shin, and E. R. Bernstein, *ibid.* **120**, 4142 (2004); (e) Y. Matsuda and E. R. Bernstein, *J. Phys. Chem. A* **109**, 314 (2005); (f) Y. Matsuda and E. R. Bernstein, *ibid.* **109**, 3803 (2005); (g) F. Dong, S. Heinbuch, S. G. He, Y. Xie, J. J. Rocca, and E. R. Bernstein, *J. Chem. Phys.* **125**, 164318 (2006); (h) S. G. He, Y. Xie, Y. Q. Guo, and E. R. Bernstein, *ibid.* **126**, 194315 (2007); (i) E. Jakubikova and E. R. Bernstein, *J. Phys. Chem. A* **111**, 13339 (2007); (j) F. Dong, S. Heinbuch, Y. Xie, J. J. Rocca, E. R. Bernstein, Z. C. Wang, K. Deng, and S. G. He, *J. Am. Chem. Soc.* **130**, 1932 (2008); (k) S. Heinbuch, F. Dong, J. J. Rocca, and E. R. Bernstein, *J. Opt. Soc. Am. B* **25**, B85 (2008); (l) Y. Xie, S. G. He, F. Dong, and E. R. Bernstein, *J. Chem. Phys.* **128**, 044306 (2008); (m) S. G. He, Y. Xie, F. Dong, S. Heinbuch, E. Jakubikova, J. J. Rocca, and E. R. Bernstein, *J. Phys. Chem. A* **112**, 11067 (2008); (n) F. Dong, S. Heinbuch, Y. Xie, J. J. Rocca, and E. R. Bernstein, *ibid.* (in press).
- <sup>41</sup> M. E. Geusic, M. D. Morse, S. C. O'Brien, and R. E. Smalley, *Rev. Sci. Instrum.* **56**, 2123 (1985).
- <sup>42</sup> M. J. Frisch, G. W. Trucks, H. B. Schlegel *et al.*, GAUSSIAN 03, Revision D.01, Gaussian, Inc., Wallingford, CT, 2004.
- <sup>43</sup> (a) L. Andrews, G. V. Chertihin, A. Ricca, and C. W. Bauschlicher, Jr., *J. Am. Chem. Soc.* **118**, 467 (1996); (b) G. V. Chertihin, W. Saffel, J. T. Yustein, L. Andrews, M. Neurock, A. Ricca, and C. W. Bauschlicher, Jr., *J. Phys. Chem.* **100**, 5261 (1996).
- <sup>44</sup> G. Balducci, G. Gigli, and M. Guido, *J. Chem. Phys.* **79**, 5616 (1983).
- <sup>45</sup> E. Murad, *J. Chem. Phys.* **73**, 1381 (1980).
- <sup>46</sup> See EPAPS Document No. E-JCPSA6-130-006910 for potential energy surfaces for  ${}^3\text{FeO}_3 + \text{CH}_3\text{OH} \rightarrow {}^3\text{FeO}_2 + \text{CH}_2\text{O} + \text{H}_2\text{O}$ ,  ${}^9\text{Fe}_2\text{O}_4 + \text{CH}_3\text{OH} \rightarrow {}^9\text{Fe}_2\text{O}_3 + \text{CH}_2\text{O} + \text{H}_2\text{O}$ ,  ${}^9\text{Fe}_2\text{O}_5$  (conformer B) +  $\text{CH}_3\text{OH} \rightarrow {}^9\text{Fe}_2\text{O}_4 + \text{CH}_2\text{O} + \text{H}_2\text{O}$ , and  ${}^9\text{Fe}_2\text{O}_5$  (conformer A) +  $\text{CH}_3\text{OH} \rightarrow {}^9\text{Fe}_2\text{O}_4 + \text{CH}_2\text{O} + \text{H}_2\text{O}$ . For more information on EPAPS, see <http://www.aip.org/pubservs/epaps.html>.